Stochastic Resonance in Graphene Bilayer Optical Nanoreceivers

Murat Kocaoglu, *Student Member, IEEE*, Burhan Gulbahar, *Senior Member, IEEE*, and Ozgur B. Akan, *Senior Member, IEEE*

***Abstract*—Graphene, a 2-D sheet of carbon atoms, is believed to have diverse application areas ranging from medicine to communications. A novel application is using graphene as a photodetector in optical communications due to its superior optical and electrical properties such as wide and tunable absorption frequency range and high electron mobility. Noise, which is especially significant in nanoscale communications, is mostly seen as an adversary. Stochastic resonance (SR) is the performance enhancement of a system due to incorporation of noise. It is shown that the excess noise in nanocommunications can be used to improve the performance of a graphene bilayer photodetector system with hard threshold decoder, when received signals are subthreshold. SR arises due to the nonlinear nature of the hard decoder. First, the SR effect due to the background ambient noise and intentional light noise is analyzed. An approximate inverse signal-to-noise ratio expression is derived, which maximizes the mutual information. The effect of frequency on the mutual information is also investigated, and it is shown that the higher frequencies are more preferable for noise limited regimes. Later, the case with the intentional noise added to the top gate is investigated. It is shown that significant mutual information improvements are achieved for subthreshold signals, due to the multiplicative stochastic terms arising from the nonlinear graphene bilayer characteristics, i.e., the exponential dependence of photocurrent on the gate voltages. All the analytical results are verified with extensive simulations.**

***Index Terms*—Bilayer graphene, graphene photodetector, mutual information, stochastic resonance (SR).**

I. Introduction

GRAPHENE, a 2-D structure with single-atomic-layer carbon atoms in a hexagonal honeycomb lattice, has popularity extending beyond physics and engineering communities [1]. Its unique mechanical, electrical, and optical properties make it even more popular than carbon nanotubes (CNTs) [2], [3]. Among its diverse potential application areas ranging from mechanical engineering to medicine, communications is one of the fields expected to benefit the most from graphene structures. With its superior electrical and optical properties, graphene could be used to develop efficient photodetectors [4]–[6]. Due to its 2-D nature, it can generate photocurrent effectively. It has a wide range of absorption frequencies and high carrier mobility. Multilayer graphene can be used to develop photodetectors with large responsivity [4], [7].

Graphene photodetectors are also strong candidates for *nanoscale communications* applications [7], [8]. Graphene's size and efficiency make it a perfect fit for nanophotodetectors. Bilayer graphene can be formed using the natural stacking fashion of graphite, i.e., Bernal stacking [9]. Although it consists of two graphene layers, bilayer graphene does not have the same properties as its single-layer counterpart. By either applying a gate voltage or chemically doping one side lifts the chiral symmetry in bilayer and opens a tunable bandgap, with new prospects of future optoelectronics components such as phototransistors [10].

The techniques to combat noise are scarce in nanoscale communications, due to the limited complexity and energy storage capabilities of nanodevices. Moreover, due to the terahertz frequency band characteristics, one of the candidate frequency bands for nanoscale communications [11], harsh molecular noise terms are added into the picture. Discovering the means to exploit noise to enhance the performance of nanoscale communication systems is thus critical. Stochastic resonance (SR) in graphene bilayer photodetectors is a way to achieve this. SR is the phenomenon of noise-induced performance enhancement of a system. Even though SR in linear systems with multiplicative noise is also reported with colored noise [12], it is mostly observed in nonlinear systems, and there is significant research work in various scenarios [13]–[15]. As indicated in [13], noise can be used to enhance signal detection at the nanoscale. In [13], the authors show via experiments that the detection performance is improved in a CNT-based transistor for several noise types. However, as far as we are aware of, no research has been conducted on SR in the graphene photodetectors.

In this study, the effects of noise in graphene bilayer photodetector are investigated and the SR potential of these devices are revealed. For the first time in the literature, artificial additive noise is applied to the incident light, thus increasing the background ambient light noise to exploit the SR in nanooptical

Manuscript received November 13, 2012; revised February 22, 2014; accepted June 25, 2014. Date of publication July 24, 2014; date of current version November 6, 2014. This work was supported in part by the Turkish Scientific and Technical Research Council (TUBITAK) under Grant #109E257, the Turkish National Academy of Sciences Distinguished Young Scientist Award Program (TUBA-GEBIP), the IBM through IBM Faculty Award. The review of this paper was arranged by Associate Editor Y.-H. Cho.

M. Kocaoglu was with the Next-Generation and Wireless Communications Laboratory, Department of Electrical and Electronics Engineering, Koc University, Istanbul 34450, Turkey. He is now with the Department of Electrical and Computer Engineering, The University of Texas at Austin, Austin TX 78712 USA (e-mail: mkocaoglu@ku.edu.tr).

B. Gulbahar was with the Next-Generation and Wireless Communications Laboratory, Department of Electrical and Electronics Engineering, Koc University, Istanbul 34450, Turkey. He is now with the Department of Electrical and Electronics Engineeringg, Ozyegin University, Istanbul 34794, Turkey and Vestel Electronics Inc., Manisa, Turkey (e-mail: bgulbahar@ku.edu.tr).

O. B. Akan is with the Next-generation and Wireless Communications Laboratory, Department of Electrical and Electronics Engineering, Koc University, Istanbul 34450, Turkey (e-mail: akan@ku.edu.tr).

Color versions of one or more of the figures in this paper are available online at http://ieeexplore.ieee.org.

Digital Object Identifier 10.1109/TNANO.2014.2339294

receivers. Furthermore, SR with additive noise at the top gate of the graphene bilayer photodetector is investigated. On contrary to the conventional optical receivers, background ambient light noise is utilized to improve the system performance. The end-to-end channel characteristics, i.e., bit crossover probabilities are derived to show that the added noise increases the mutual information in the optical transmitter/receiver system. An approximate analytical noise power expression that maximizes the mutual information for a given subthreshold signal is obtained. Moreover, effects of the frequency on the mutual information are investigated. Finally, it is shown that the intentional top-gate noise can be used to increase the mutual information. In both cases, performance can significantly be improved.

The paper is organized as follows: In Section II, the relevant work on graphene photodetectors and SR are revealed. In Section III, the system model is explained. Section IV is devoted to the derivation of the bit switching probabilities to investigate the variation of the mutual information at the threshold-based nanoscale photodetector, and approximate noise power expression for the optimum mutual information. The effects of the signal frequency are also investigated. Numerical evaluations of the analytical expressions and simulations to verify the assumptions are conducted in Section V. This paper is concluded in Section VI.

II. Related Work

The use of graphene as ultrafast photodetectors is first investigated in [6], considering single- and a few-layered graphene, to conclude that the unique properties of graphene, such as very small band gap and high mobility make it an efficient photodetector. In our previous work [7], we develop a communication theoretical framework for modeling single-layer graphene photodetectors. Experimental demonstration of the graphene photodetectors is first conducted in [16] to show the promise of graphene in communications field. In [4], the authors develop analytical models of graphene bilayer phototransistor (GBL-PT)-based photodetectors and develop responsivity and detectivity expressions. GBL-PTs surpass the quantum well and quantum dot infrared (IR) photodetectors due to the large quantum efficiency and photoelectric gain. Similarly, in [17], the authors develop the device model, and responsivity and detectivity expressions for the multiple graphene-layer photodiode-based terahertz and IR detectors.

SR occurs in nonlinear systems as the enhancement of system performance due to incorporation of noise and has a considerable literature. In [18], the authors consider a summing array of N comparators. They conclude that, for uniform and Gaussian signal and noise, transmitted information is maximized at a nonzero noise level when thresholds are set to the mean of the signal, which they term as suprathreshold SR. In [14], many noise distributions are shown to induce SR in threshold neurons, and optimal noise levels for these distributions are derived. In [15], the optimal threshold distributions in noisy threshold devices are investigated considering the SR effect. In nanodomain, the authors in [13] demonstrated the SR effect in CNTs experimentally, evaluating metrics of mutual information, cross correlation, and inverted bit error rate. They conclude that the CNTs exhibit SR effect in various noise types and could be used to detect subthreshold signals.

Despite these, SR in graphene photodetectors is not yet investigated. Noise is exploited in graphene photodetectors, where only bilayer graphene photodetectors are considered due to their simplicity and performance similar to the multilayer counterparts. Moreover, bilayer graphene is expected to surpass single-layer graphene in terms of the optical detection.

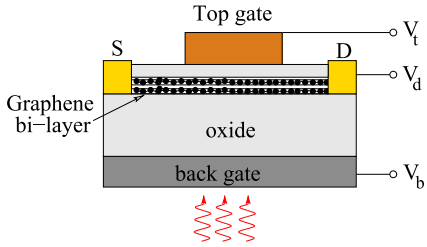

Fig. 1. Bilayer graphene photodetector.

III. System Model

In this section, the details of the graphene bilayer photodetector are provided, and the signal model and the detection mechanism at the nanoscale receiver are explained; input–output relation in terms of the mutual information is obtained.

A. Graphene Bilayer Photodetector Model

The graphene bilayer photodetector shown in Fig. 1 has four gates called the *top, back, source,* and *drain gates*. Its characteristics are investigated in detail in [4], and the relation between photocurrent, incident light power, and gate voltages are derived. The incident optical signal induces photocurrent $I_{\rm ph}$ in the graphene photodetector written as [4]

$$I_{\rm ph} = RX_s + n_d + n_T. \tag{1}$$

In (1), R is called the responsivity, which is an important efficiency metric for the photodetector since it determines the photogenerated current for a given received optical power level. Apart from the constant terms, responsivity depends on the optical frequency, top, back, and drain gate voltages, when source gate is grounded. Derived in [4], responsivity is

$$R = \frac{\xi}{\omega}\Theta(\hbar\omega - \hbar\omega_{\rm off})\exp\left(\frac{a_B}{8W}\frac{qV_b}{k_BT} + \frac{d}{2W}\frac{qV_t}{k_BT}\right)\left(\frac{1-\exp(-qV_d/k_BT)}{1+\exp(-qV_d/k_BT)}\right) \tag{2}$$

where ω is the optical signal frequency, and V_b, V_d, and V_t are back, drain, and top gate voltages, respectively. $\xi = (8\,q\,L_t\,\beta\,W\,\alpha)\,/\,((L_t+2L_c)\beta_c\,a_B\,\hbar)$ is a constant, and $\Theta(\hbar\omega) = 1/2 + (1/\pi)\tan^{-1}(\hbar\omega/\gamma)$ is the unity step function with smearing γ, e.g., 2 meV. The other constant terms in (2) and expressions of $\Theta(\hbar\omega)$ and ξ are given in Table I. The term $\hbar\omega_{\rm off} = qd(V_b - V_t)/2W$ is the photon cutoff energy. Therefore, the optical frequency should exceed $\omega_{\rm off}$.

TABLE I
PARAMETER DEFINITIONS

Parameter	Definition	Value
q	Electron charge	1.6E-19 C
d	Spacing between graphene layers	0.36 nm
W	Thickness of layers between graphene/gates	20 nm
a_B	Bohr radius	4 nm
ε_r	Dielectric constant	0.35
m	Effective mass of electrons/holes in graphene	2.83E-13 eVs^2/m^2 [19]
$\hbar$	Planck constant	6.58E-16 eVs
k_B	Boltzmann constant	8.617E-5 eV/K
T	Temperature	300 K
L_t	Length of the top gate	300 nm
L_c	Length of the source and drain sections	300 nm
β_c	Fraction of injected holes passing to source and drain	0.033
α	Universal graphene absorption constant	$2\pi/137$
β	Fraction of injected electrons passing to gated section	0.1

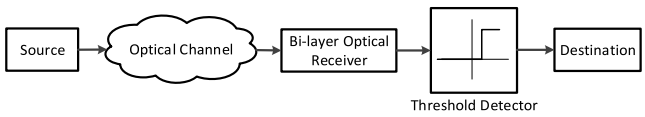

Fig. 2. Communication system model.

X_s in (1) is the optical power intensity at the receiver. n_d is the dark current noise term, and it can be assumed zero-mean Gaussian with variance σ_d^2 such that $\sigma_d^2 = 4\,q\,g\,J_0\,B$, where g is the photoelectric gain (see (18) in [4]), B is the operational bandwidth (100 MHz), and J_0 is the dark current in the bilayer graphene photodetector given in [4] as

$$J_0 = \beta \frac{q\sqrt{2m}(k_B T)^{3/2}}{\pi^{3/2}\hbar^2} \left(1 - \exp\left(\frac{-qV_d}{k_B T}\right)\right) \left(\exp\left(\frac{a_B}{8W}\frac{q\,(V_b)}{k_B T}\right) - 1\right) \times \exp\left(\frac{q\,(V_b + V_t)}{2k_B T}\right). \quad (3)$$

Thermal noise term, i.e., n_T, is also zero-mean Gaussian and its variance can be written as $\sigma_T^2 = 4\,k_B\,T\,B\,R_{eq}$ [7], where R_{eq} is equivalent resistance for graphene and is taken as $R_{\text{eq}} = 50\Omega$ in general, assuming that the equivalent resistance is determined by the load, which is much smaller than the internal resistance of the bilayer graphene [9].

B. Receiver Modeling

One of the most important parameters to consider for nanoscale communications is the low complexity requirement. The incredibly tiny nanodevices cannot perform complex operations, such as maximum likelihood detection. Hence, a hard threshold decoder is assumed at the receiver, suited for nanocommunication applications due to its simplicity. The hard threshold decoder announces received symbol as 0 bit if it is below the threshold and as 1 bit otherwise. Thus, the input–output relation of a hard threshold decoder is nonlinear. The generated photocurrent is compared with a predefined threshold to determine the received symbol. The system model is provided in Fig. 2. Source generates the binary, independent, and identically distributed bit stream at the transmitter. These source symbols are mapped to the modulated channel symbols. To satisfy the energy efficiency requirement at the nanoscale, ON–OFF keying (OOK) modulation, and its variants are proposed for nanoscale communications together with new channel code designs [11], [20], [21]. If no noise were introduced by the channel, the power of the received signals would be $X_s \in \{X_0, X_1\}$, corresponding to 0-bit and 1-bit symbol, respectively. One would expect $X_0 = 0$ and $X_1 = P$ due to OOK modulation. Assuming a binary symmetric optical channel, the threshold of the detector, i.e., I_{th} is set to $I_{\text{th}} = I_1/2$ for the optimal detection, where I_1 is the photogenerated current when the photodetector receives signal power of P. Therefore, from (1), $I_{\text{th}} = \text{RP}/2$.

Due to the noisy and unstable nature of the communication channel, the received signal might be below threshold, although 1 bit is sent from the transmitter. This behavior is expected to occur more frequently in nanoscale communications than the classical communications, since the nano-communication channel is less reliable and more dynamic. These type of signals are called the *subthreshold* signals. The power of the subthreshold signals at the receiver are represented by $X_s = P/k,\ k > 2$. k is called the *subthreshold coefficient*. The bits associated with the subthreshold signals can be called in "erasure" at the receiver. Assume that the receiver has the perfect knowledge of the times that the received symbol is subthreshold. Decoding a subthreshold signal directly is not desirable, since correct decision is highly unlikely. If there is a feedback link available from receiver to the transmitter, transmitter could request retransmission for the erased bits. However, in nanoscale communication scenarios, no feedback link exists due to the complexity and energy constraints. Exploiting this inherent noise via SR phenomenon in bilayer graphene photodetectors is proposed to enhance the receiver performance. With SR, the amount of information that can be extracted from the subthreshold signals is increased. Since hard threshold decoding is a nonlinear system, SR is expected to occur in the considered scenario with subthreshold received signals.

Two main scenarios are considered: the effect of the incident light noise (background noise) and the effect of the top-gate noise. In accordance with the communication theory, noise at the receiver is modeled as additive noise on both incident light

and the top-gate voltages. Incident light noise brings an additive term to the overall photocurrent, similar to the existing SR studies. It is shown that there is an optimum intentional noise level depending on the background noise level, which maximizes the mutual information via SR effect, which is the first SR analysis in this setting. The photocurrent characteristics of the graphene photodetector offer a new form of SR for the top-gate noise. Noise added to the top gate affects the photocurrent multiplicatively, since photocurrent of the graphene photodetector depends on the top-gate voltage exponentially as shown in (3), instead of the classical additive noise. As a result, the generated photocurrent becomes a random variable with characteristics depending on the noise added to the top gate. If it is Gaussian, photocurrent becomes a log-normal random variable. The probability density functions (PDFs) of the generated photocurrent are derived for both cases.

C. Information Theoretical Modeling of the Nanoreceiver

The fundamental metric to be investigated is the mutual information since it is more robust compared to the other parameters, such as the signal-to-noise ratio (SNR). Mutual information between the transmitted symbol X and the received symbol Y is given by $I(X;Y) = H(Y) - H(Y|X)$ [22]. $H(X)$ is the well-known information-theoretic entropy of the discrete random variable X. The end-to-end communication channel is modeled as a binary asymmetric channel (BAC). p_{01} and p_{10} are the bit switching probabilities when 1 and 0 are transmitted, respectively. Since hard threshold decoding is applied, the crossover probabilities depend on the distribution of the received signal. Equiprobable source symbols are assumed as previously stated, which is well justified by the Shannon's source-channel separation theorem [22]. The bit switching probabilities of the BAC are given as follows:

$$p_0^y = (p_{00} + p_{01})/2, \;\; p_1^y = (p_{11} + p_{10})/2 \tag{4}$$

where $p_i^y = p(Y = i)$, $i \in \{0, 1\}$ and $p_{ji} = p(Y = j, X = i)$, $i, j \in \{0, 1\}$. The mutual information is

$$H(Y) = -p_0^y \log p_0^y - p_1^y \log p_1^y \tag{5}$$

where logarithm is in base 2. $H(Y|X)$ can be expressed as

$$H(Y|X) = 0.5H(Y|X = 0) + 0.5H(Y|X = 1) \tag{6}$$

where $H(Y|X = i) = -p_{0i} \log p_{0i} - p_{1i} \log p_{1i}$.

Bit error probability is also evaluated in addition to the mutual information by the expression $P_e = 0.5(p_{01} + p_{10})$ due to the equiprobable source. Bit switching probabilities are calculated for two cases, namely in the presence of incident light noise and top-gate noise. It is shown that the mutual information increases with the incorporation of noise for subthreshold received signals, both by evaluation of analytical expressions and extensive simulations.

IV. SR in Bilayer Graphene Nanoreceivers

In this section, the effects of various noise terms on the performance of the graphene bilayer optical nanoreceiver are investigated. First, the Gaussian noise is added to the incident light in addition to the existing ambient background light noise. This is a highly practical scenario due to the noisy nature of the nanoscale-communications channel. The squared magnitude of the added noise term contributes to the incident light power. Second, the effects of the additive top-gate noise at the graphene photodetector are analyzed. Different from most of the existing SR studies, exponent of the noise term is multiplied with the received symbol due to exponential dependence of the bilayer graphene photocurrent on the top-gate voltage (3). However, the physical structure of the photodetector imposes limits on the maximum noise; hence, maximum benefit can be obtained from the top-gate noise. In the rest of this paper, PDFs of the functions of the random variables are calculated as follows [23]:

$$f_Y(y) = \frac{f_X(g^{-1}(y))}{|dg(x)/dx|_{x=g^{-1}(y)}} \tag{7}$$

where $y = g(x)$ and PDFs of x and y are $f_X(x)$ and $f_Y(y)$, respectively. To use the relation in (7), the function g must be strictly monotonic. All the relations used throughout this paper satisfies this requirement in the considered range of values. Deriving the PDF of the generated photocurrent from the noise distribution is a fundamental step to evaluate the performance enhancement of graphene photodetectors with SR.

A. SR With Incident and Ambient Light Noise

Noise is mostly seen as an adversary for optical communication systems. For example, in IR communications, sunlight and fluorescent lamps are common noise sources [24]. In the presented setting, the noise is exploited to enhance the performance of an optical communication system. Intentional light sources such as laser or LED can be used at either the receiver end or by an assistant node to insert the required amount of noise adaptively.

The probability $p(I_{\rm ph} < I_{\rm th})$ for the subthreshold signal is needed. Consider the signal model given in (1). Background noise contributes to the incident light power, X, leading to

$$I_{\rm ph} = R(X_s + n_i^2) + n_d \tag{8}$$

where n_i^2 is the instantaneous power of the background noise, which is assumed to be Gaussian. Notice that instead of the average power, the instantaneous power at the receiver, i.e., n_i^2 is used, and this allows us to observe the SR effect, which can be exploited to improve the overall system performance as it is shown in the subsequent sections. The probability distribution of the photocurrent is derived next, in order to reveal the effects of the background noise on bit switching probabilities. Notice that the thermal noise term of (1) in (8) is ignored. In the following, when there is noise added to the incident light, the effect of the dark current is also ignored. This assumption will later be verified by comparing the evaluation of the analytical expressions with the simulation results in Section V. Then, the following is obtained:

$$p(I_{\rm ph} < I_{\rm th}) = p(RX_s < I_{\rm ph} < I_{\rm th}) \tag{9}$$

$$= p(0 < Rn_i^2 < I_{\rm th} - RX_s) \tag{10}$$

since n_i^2 is always positive. The bit switching probabilities are

$$p_{01}= p(I_{\rm ph} < I_{\rm th}|X_s = P),\ p_{10} = 1 - p(I_{\rm ph} < I_{\rm th}|X_s{=}0) \tag{11}$$

where p_{10} (p_{01}) is the probability to decode the received signal as 1 (0), when the transmitted bit is 0 (1).

Let $I_n = g(n) = Rn^2$. I_n is the stochastic current generated at the photodetector due to the background noise. Using (7) and considering the fact that $i > 0$, the PDF of I_n is

$$f_{I_n}(i) = \frac{1}{\sqrt{2\pi\sigma^2 Ri}} e^{-\frac{i}{2\sigma^2 R}} \tag{12}$$

which is the gamma distribution of the type

$$f_{I_n}(i) = \frac{1}{\Gamma(k)\theta^k} i^{k-1} e^{-\frac{i}{\theta}} \tag{13}$$

with $k = 1/2$ and $\theta = 2\sigma^2 R$, where σ is the standard deviation of the background noise. Then, the probability $p(0 < I_n < I_{\rm th} - RX_s)$ is obtained from the cumulative distribution function of the gamma distribution as

$$p(0 < I_n < I_{\rm th} - RX_s) = \ {\rm erf}\left(\sqrt{\frac{I_{\rm th} - RX_s}{2\sigma^2 R}}\right)$$

$$\Rightarrow p_{01} = \ {\rm erf}\left(\sqrt{\frac{P}{2\sigma^2}\left(\frac{1}{2} - \frac{1}{k}\right)}\right). \tag{14}$$

Similarly, from (11), p_{10} is given as

$$p_{10} = 1 - p(0 < I_n < I_{\rm th}) = {\rm erfc}\left(\sqrt{\frac{P}{4\sigma^2}}\right). \tag{15}$$

Interestingly, both crossover probabilities do not depend on the responsivity of the photodetector for the subtheshold signals. Evaluation of the analytical expressions and also verification with simulations are presented in Section V. It is shown that there is an optimal noise power level for a given signal power that maximizes the mutual information. As the theoretical optimum is hard to find, an approximate noise power to signal power ratio, i.e., inverse SNR (ISNR) expression is derived that shows significant information gains. For any subthreshold coefficient k, the following ISNR provides significant improvements in terms of the mutual information

$$\left(\frac{\sigma^2}{P}\right)^* = \frac{1}{k}[\ln k - \ln(k-2)]^{-1}. \tag{16}$$

Derivation of (16) is provided in the Appendix. Using this expression, a simple adaptive algorithm is proposed to maximize the mutual information using SR in dynamical environments.

1) Adaptive Noise Algorithm: The incident light noise is mainly due to the background noise in the optical communication channel. As indicated before, there may be other noise sources such as fluorescent lamps or daylight to contribute to the background noise. Therefore, the incident light noise process is time varying as represent by $n_i(t)$. At any time instant, depending on the subthreshold coefficient k and the signal power $P(t)$, there is an optimal noise power that maximizes the mutual information, which is approximated by (16) as $P_n^*(t) = P(t) * \frac{1}{k}[\ln k - \ln(k-2)]^{-1}$. If the time instants for the subthreshold signals and the subthreshold coefficients are known with the background noise of $P_b(t)$, intentional incident noise with power of $P_{\rm in}(t) = P_n^*(t) - P_b(t)$ can be injected to the communication channel to assure that the noise power is kept at the optimal value. Therefore, Algorithm 1 can be employed at each time slot to maximize the photodetector system performance by introducing intentional noise. The threshold detection is shown by the indicator function $\mathbb{1}(RX_s > I_{\rm th})$. Note that this algorithm can run at either the receiver or at an assistant node, which has access to channel information and knows the transmitter power *a priori*. Then, insertion of the Gaussian noise $\mathcal{N}(0, \sqrt{P_{\rm in}})$ to the channel helps nanoreceiver to encode higher amount of information.

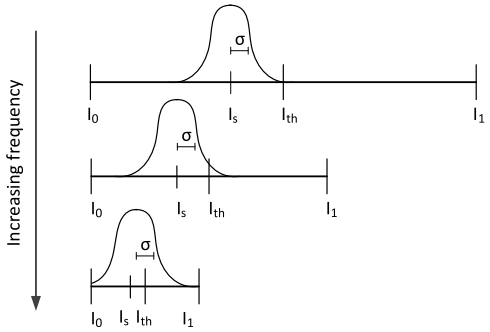

Fig. 3. Illustration of the effect of frequency variation on the signal levels.

Algorithm 1: Adaptive Stochastic Resonance Algorithm

Input: X_s, R, I_{th}, P_b
if *signal not subthreshold* **then**
  do $Z = \mathbb{1}(RX_s > I_{th})$
else
  Detect sub-threshold coefficient k
  Find P_n^* from (16)
  Find $P_{in} = P_n^* - P_b$
  $X_s \Leftarrow X_s + n_{in}^2$, $n_{in} \sim \mathcal{N}(0, \sqrt{P_{in}})$
  do $Z = \mathbb{1}(RX_s > I_{th})$
end
Output: Z

2) Effect of Optical Frequency on SR: The above analysis is evaluated in Section V for a fixed signal frequency of $\omega = 25$ THz. The effect of the frequency variation on mutual information is also investigated, in low- and moderate-noise scenarios. From (1), the responsivity of the photodetector depends on frequency. It can be easily seen that the responsivity of the photodetector decreases with increasing frequency, in general. However, as obtained in (14) and (15), with the assumptions of no dark and thermal current noise, the crossover probabilities do not depend on the responsivity. Therefore, the mutual information is independent from the frequency under these assumptions. However, when the effect of dark and thermal current noise terms is incorporated, a different behavior arises. Consider Fig. 3, where σ^2 is the total Gaussian noise power at the photodetector with dark current and thermal noise components. In the first subfigure, it is observed that the added noise is not sufficient

to observe SR effect, since probability that the received signal exceeds the threshold $I_{\rm th}$ is 0 (assuming the tail of Gaussian is negligible beyond $I_{\rm th}$). If frequency is increased, responsivity of the photodetector decreases, transforming the signal levels as in the second figure, i.e., closing the gap between subthreshold signal with the same subthreshold coefficient and the threshold due to the scaling of the signals. As observed, the same amount of noise induces nonzero correct decoding probability of the subthreshold signal now, since probability that the signal is beyond the threshold is nonzero. Hence, mutual information increases with frequency via responsivity. However, if frequency increases more such that the probability of the subthreshold signal being decoded as 1 approaches 0.5, mutual information decreases. Hence, there is an optimal operation frequency for each noise power and subthreshold coefficient. This behavior is observed in Section V and explained in detail. It is concluded that the mutual information does not only depend on the incident light noise power, but also on the dark current noise and thermal noise, which can be exploited to increase the mutual information at higher frequencies.

B. SR With Top-Gate Noise

In this section, the addition of intentional noise to the top gate is considered, allowing more control on the noise distribution, unlike the existing ambient noise in the noisy incident light scenario. At this point, it is important to underline that the expressions and derivations in [4] are valid only if the gated section is fully depleted, which requires that $V_{\rm th}^* < V_t < V_{\rm th}$. Following [4], $V_t = V_{\rm th}^*$ is assumed. Therefore, the top-gate noise of the graphene bilayer photodetector should not take values outside the interval $[0, V_{\rm th}–V_{\rm th}^*]$. The most intuitive distribution satisfying this is the uniform distribution. Hence, the effect of incorporating uniform noise to the top-gate voltage is investigated first. Second, the Gaussian noise is considered, which is the noise type mostly encountered and that can easily be obtained from natural phenomena.

If $h\omega \gg qdn_t/W$ is assumed, the generated photocurrent is

$$I_{\rm ph} = I_0 e^{Cn_t} \tag{17}$$

where I_0 is the current without incorporation of noise, and C is the multiplicative factor of V_t in the exponential term in (1), i.e., $C = qd/(2Wk_BT) \approx 0.35$ at room temperature, i.e., $T = 300\,^\circ$K. Let the function mapping n_t to $I_{\rm ph}$ be $I_{\rm ph} = g(n_t)$. PDF of the photocurrent with additive top-gate noise, i.e., $I_{\rm ph}$, can be derived from the PDF of n_t using (7).

1) Uniform Noise: Assume that the top-gate noise is uniformly distributed. In order to satisfy the requirement $V_{\rm th}^* < V_t < V_{\rm th}$, n_t is uniformly distributed by $n_t \sim U[0, T]$, where $T \leq V_{\rm th} - V_{\rm th}^* = 2V_b d/W$. The dark current noise and the thermal noise is assumed to be low, i.e., $\tilde{I}_{\rm ph} = I_{\rm ph}e^{Cn_t} + n_d + n_T \approx I_{\rm ph}e^{Cn_t}$, where $I_{\rm ph} = {\rm RP}/k$ with $k > 2$ for the subthreshold signal. This assumption significantly simplifies the analysis, since PDF of the received current can then be easily derived without the need for convolution, and it is validated with simulations in Section V. However, the dark current noise and thermal noise are incorporated into the crossover probability calculation of 0 bit. When 0 bit is transmitted, i.e., $X_s = 0$, only these additive noise terms affect the generated current from (1). Let $\tilde{I}_{\rm ph} = g(n_t)$. From (7)

$$f_{\tilde{I}_{ph}}(i) = \begin{cases} 1/{\rm CT}i, & I_{\rm ph} < i < I_{\rm ph}e^{\rm CT} \\ 0, & \text{otherwise.} \end{cases} \tag{18}$$

Obtained PDF can be used to determine the bit switching probability from 1 to 0, i.e., p_{01}

$$p_{01} = p(\tilde{I}_{\rm ph} < I_{\rm th}) \tag{19}$$

$$= \begin{cases} 0, & I_{\rm ph}e^{\rm CT} < I_{\rm thr} \\ \frac{1}{\rm CT}\log\left(\frac{I_{\rm thr}}{I_{\rm ph}}\right), & I_{\rm ph} < I_{\rm thr} < I_{\rm ph}e^{\rm CT} \\ 1, & I_{\rm thr} < I_{\rm ph} \end{cases} \tag{20}$$

where $I_{\rm thr}$ is the threshold current. Similar to previous section, the threshold current is set to $I_{\rm th} = {\rm RP}/2$ and photocurrent due to subthreshold signal is $I_{\rm ph} = {\rm RP}/k$. Then, simplifying (19) in the suitable range for $I_{\rm th}$

$$p_{01} = \frac{1}{\rm CT}\log\left(\frac{k}{2}\right). \tag{21}$$

Bit switching probability for 0 bit, i.e., p_{10}, can be simply found using the Gaussian dark current and thermal noise variances as

$$p_{10} = 0.5\left(1 - {\rm erf}\left(\frac{I_{thr}}{\sqrt{2(\sigma_d^2 + \sigma_t^2)}}\right)\right) \tag{22}$$

where σ_d^2 is the dark current noise and σ_t^2 is the thermal noise. Note that the dark current noise depends on the value of the top-gate voltage. However, for simplicity, the dark current noise is taken as if no noise is added to the top gate. It is later shown that such an approximation is acceptable for the range of top-gate noise values. Since noise contributes to the current multiplicatively, the added noise does not increase p_{10} unlike the classical SR scenarios. Therefore, excessive noise provides significant gains due to the graphene bilayer characteristics, since bit crossover probability p_{10} does not increase with the incorporation of top-gate noise. The variation of mutual information can be obtained using the crossover probabilities obtained in (19) and (22).

2) Gaussian Noise: Assume that the noise added to the top gate is Gaussian distributed. In order to satisfy the voltage range required for the top gate, it is assumed that $Pr\{n_t > n_0\} \approx 0$, if $n_0 \geq 3\sigma$, where σ is the standard deviation of the distribution. Therefore, the scope is limited to the noise class $n_t \sim \mathcal{N}(3\sigma, \sigma^2)$, where $\sigma \leq T/6$. Again, the dark current and the thermal noise terms are ignored, when the received symbol is 1. PDF of the photocurrent is

$$f_{I_{\rm ph}}(i) = \frac{1}{i\sqrt{2\pi\tilde{\sigma}^2}} e^{-\frac{(\log i - \tilde{\mu})^2}{2\tilde{\sigma}^2}} \tag{23}$$

where $\tilde{\sigma} = C\sigma$ and $\tilde{\mu} = \log I_{ph} + C\mu$ as used in Section IV-B, and $\mu = 3\sigma$ is the mean of the Gaussian noise. The bit crossover probability p_{01} is

$$p_{01} = 0.5\left(1 + {\rm erf}\left(\frac{\log I_{\rm thr} - \tilde{\mu}}{\sqrt{2\sigma^2}}\right)\right). \tag{24}$$

Since the effect of noise added to the top gate on the dark current noise is ignored, p_{10} is the same as given in (22). Using p_{01}, p_{10} and assuming equiprobable source symbols, mutual information is obtained by entropy of output symbol y, i.e., $H(Y)$, and equivocation of the channel using the crossover probabilities, i.e., $H(Y|X)$ by $I(X;Y) = H(Y) - H(Y|X)$. In Section V, the bit switching probabilities are evaluated and the results are compared with simulations.

V. Simulations and Numerical Analysis

In this section, the numerical evaluations and simulations of the performance enhancements in graphene bilayer photodetectors conducted in MATLAB are presented. Equations (1) and (8) are used and the Gaussian and normal distributed random variables are incorporated, and the numerical evaluations of the mutual information as a function of several parameters are performed. The theoretical average bit error probability and the mutual information are calculated for the BAC using the obtained bit crossover probabilities in Section IV and expressions in Section III-C. Later, simulations are performed to validate the approximate analytical expressions.

The solid curves in Figs. 4, 6, and 7 show the numerical evaluations of analytical expressions, whereas the dashed curves yield the simulation results. In each simulation experiment, a large number of (100 000) noise samples are obtained with the desired noise distribution. Later, the bit crossover probabilities are calculated using the law of large numbers as

$$p_{01} = \frac{\text{\# of bits below the threshold}}{\text{Number of total bits}}$$

$$p_{10} = \frac{\text{\# of bits exceeding the threshold}}{\text{Number of total bits}}$$

where received power is kept at $X_s = 0$ for p_{10} and $X_s = P/k$ for p_{01} calculation, where k is the subthreshold coefficient as explained previously. The signal frequency is taken $\omega = 2.5$ THz in order to satisfy the condition $h\omega \gg qdn_t/W$ in the simulations in Figs. 4, 6, and 7.

A. Incident Light Noise

Fig. 4 shows the variation of mutual information and bit error probability, when noise is added to the incident light. The detection threshold is set to $\mathrm{RP}/2$, whereas the received signal is P/k for fixed R. Variation of k from 2.01 to 2.12 is shown with steps of 0.01. It is trivial that the smaller the k value, the closer the received signal gets to the threshold from left, leading to greater gains. As received signal fades more and more, the gain obtained from the incident light noise diminishes. The x-axis shows the ratio of the noise power to signal power, i.e., ISNR. As observed, one can find an optimal noise power for each k, at which mutual information is maximized. For small k values, the enhancement is significant as observed. From Fig. 4(a), for $k = 2.01$, 65% of noise-free communication rate can be achieved with the addition of noise with 0.07 times the signal power. Simulation results closely follow the theoretical curves and show the validity of ignoring the effects of the dark and thermal noise terms in the analysis. The approximate σ^2/P obtained analytically in (16) to yield the maximum mutual information in Fig. 4(a) is also indicated with downside triangles. As shown, the approximate ISNR expression provides mutual information close to the maximum, without the need to use any approximation algorithms.

As incident light is initially assumed noise free, the observed optimum noise power reflects the total power accompanying the optical signal. Therefore, the existing background ambient noise should be subtracted from the optimal noise power to obtain the required intentional power value. If the environment is dynamic, with time varying ambient background noise, the adaptive algorithm presented in Section IV-A could be employed to provide significant enhancements.

The effect of frequency on the mutual information is also investigated, where two noise cases called *low-noise* and *moderate-noise* scenarios are considered. In the low-noise regime, $\mathrm{SNR} = 1000$, and in the moderate-noise regime $\mathrm{SNR} = 10$. Fig. 5(a)–(c) shows the variation of mutual information with varying frequency for these two cases for $k = 2.01$, $k = 2.05$, and $k = 2.12$, respectively. In Fig. 5(a), i.e., for $k = 2.01$, it is observed that the mutual information slightly increases at first, and then starts to decrease, for the moderate-noise regime. Therefore, it can be concluded that p_{11} approaches to 0.5 as frequency is increased, as explained in detail in Section IV-A. However, in the low-noise regime, increasing the frequency increases the mutual information, since p_{11} increases from 0, leading to SR effect in the photodetector. It is observed in Fig. 5(b) and (c) that, as the subthreshold coefficient increases, the effect of noise decreases. Therefore, decrease of responsivity with increased frequency is required for the same amount of noise to create significant SR effect for the signals with high subthreshold coefficient. This analysis suggests that, if the dark current and the thermal noise are insufficient to create SR effect, the detection performance at higher frequencies is improved. The practical limitation to this, which is not considered in this study, is that the detection becomes harder as the frequency is increased, since signal levels become closer as illustrated in Fig. 3. Therefore, the best frequency to yield the maximum mutual information should be lower than the results obtained in this theoretical study, due to the errors introduced by the threshold detection system.

B. Top-Gate Noise

Mutual information and bit error probability are observed with top-gate noise at the photodetector. The detection threshold of the system is set to $\mathrm{RP}/2$, and the received signal is P/k as in Section V-A. However the responsivity, i.e., $\tilde{R} = \tilde{R}(n_t)$, is stochastic due to the noise n_t added to the top gate. Uniform and Gaussian noises are considered next.

1) Uniform Noise: Fig. 6 shows the performance enhancement of the receiver, when uniformly distributed n_t, i.e., $n_t \sim \mathcal{U}[0, T]$ is added to the top gate. x-axis shows $V_t + \max\{n_t\}$, i.e., the maximum top-gate voltage that can be observed due to noise. This metric is important, since it should be below a certain threshold for the conduction channel to form in the bilayer graphene. Hence, the performance gain that can be obtained with noisy top gate is limited due to the physical structure of graphene bilayer photodetector. As shown in Fig. 6, top-gate noise

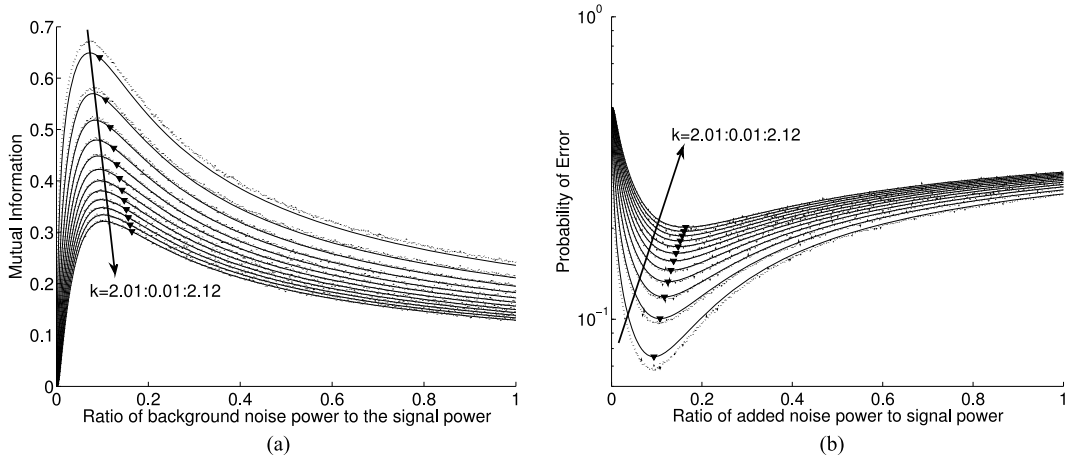

Fig. 4. Variation of mutual information and error probability with different Gaussian noise powers. x-axis shows the ratio of noise power to the signal power, i.e., P_n/P. Analytical approximation results are indicated with downside triangular markers.

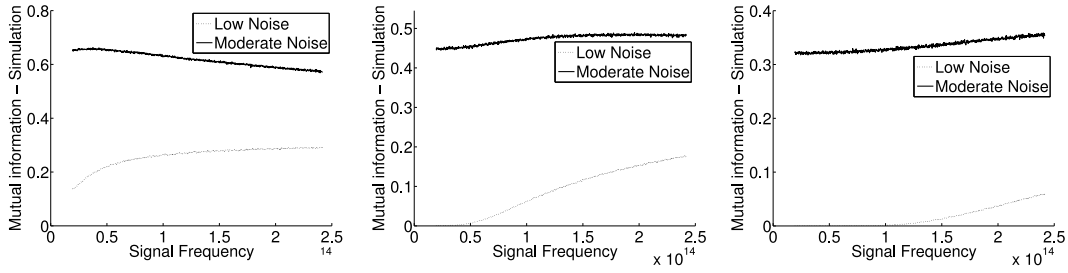

Fig. 5. Mutual Information versus incident light frequency for varying k. (a) $k = 2.01$. (b) $k = 2.05$. (c) $k = 2.12$.

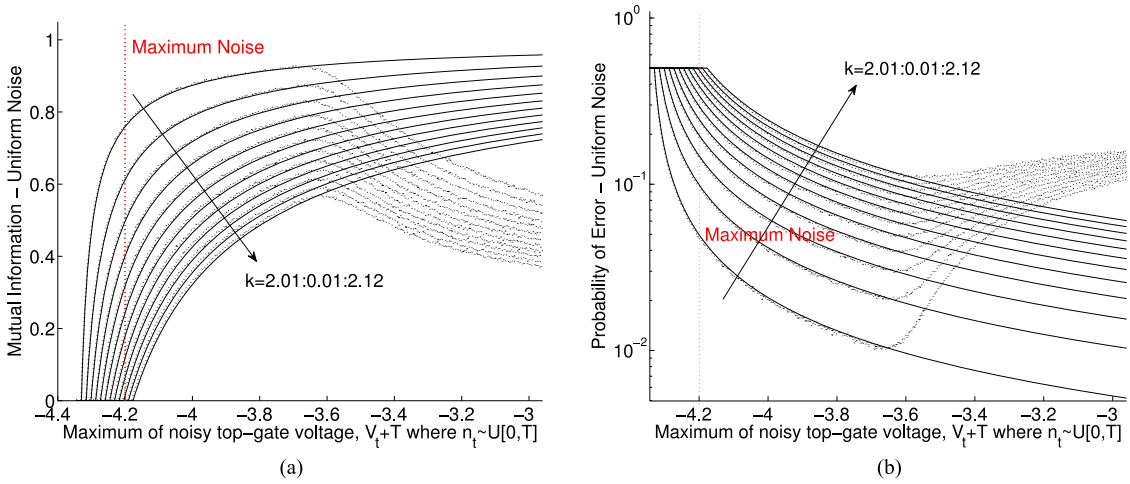

Fig. 6. Variation of mutual information and error probability with different uniform top-gate noise values.

provides significant performance enhancement, when sub-threshold signals are received. The horizontal red line shows the limiting voltage value for the top gate. Therefore, only the performance enhancements obtained on the left-hand side of this line can be achieved. The theoretical results on the right-hand side cannot be achieved, since the photocurrent expressions become invalid in this range. As observed from the dashed curve, the maximum information gain cannot be achieved due to this limit, which is on the right of the maximum top-gate voltage. It is clear that significant gain is obtained with the addition of noise if $k < 2.1$.

Simulation experiments are conducted by calculating the dark current noise and photocurrent using the noisy top-gate voltage, leading us to observe the validity of our approximations in the analytical calculations. An important point is that the analytical expressions and simulation results deviate after a certain

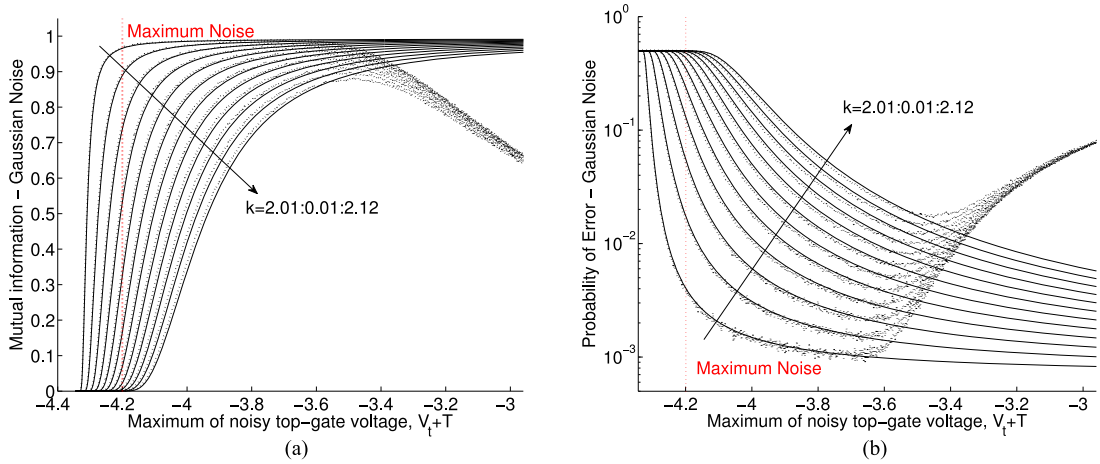

Fig. 7. Variation of mutual information and error probability with different Gaussian top-gate noise values.

maximum top-gate voltage value due to the assumptions. One reason for the deviation from the analytical results is that noise starts to increase p_{10} after some point, which is not the case in the analytical evaluations, since the effect of added noise in the expression for the dark current noise is ignored. However, as clearly shown in Fig. 6, the analytical expressions provide an almost perfect fit with the simulation results for the feasible region. Therefore, the assumptions and the analysis are acceptable for the range of noise values suitable for the graphene bilayer photodetector. The deviation from the theoretical results is never observed, since adding noise greater than *the maximum allowed noise level* is physically impossible, as it will push the bilayer graphene out of the conduction band.

2) Gaussian Noise: Fig. 7 shows the variation of mutual information for different values of $V_t + \max\{n_t\}$. As indicated in the previous sections, in order to assure that V_t is within the required limits, n_t is selected as Gaussian distributed with mean $\mu = 3\sigma = \frac{V_{\rm th} - V_{\rm th}^*}{2}$ and standard deviation σ, i.e., $n_t \sim \mathcal{N}(3\sigma, \sigma)$. As a result, the probability that the top-gate voltage exceeds the allowed limits becomes less than 2%. As observed in Fig. 7, mutual information approaches very close to 1, for small k values. Therefore, the mutual information benefits more from the Gaussian noise than the uniform noise. This is expected, since the PDF of the Gaussian distribution is more concentrated and most of the time it pulls the photocurrent above threshold, whereas the uniform noise has significant probability of falling below the threshold.

VI. Conclusion

In this paper, effects of the intentional noise on the graphene bilayer photodetector performance are investigated. Incorporating noise to enhance the system performance can be effectively used in nanoscale communications due to the excessive amount of noise resulting from the highly dynamical nature of the nanocommunication channel. The mutual information and error probability metrics are used to evaluate the system performance. Significant performance gains can be achieved through incorporation of noise with sufficient power. It is shown that it is not possible to achieve the optimum mutual information gains via top-gate noise addition, due to the limiting physical structure of the bilayer graphene phototransistor. On the other hand, an adaptive algorithm can be employed to maximize the mutual information by injecting a suitable amount of noise on the incident light by an assistant node or by the receiver to maximize the mutual information, when subthreshold signal is detected. An approximate ISNR expression is derived, which maximizes the mutual information for any subthreshold coefficient. The effective use of noise as demonstrated in this paper can lead to novel nano or classical graphene-based optical communication systems.

Appendix
Derivation of ISNR Expression in (16)

The mutual information for the BAC with equiprobable source outcomes can be expressed as

$$I(X;Y) = H\left(\frac{1 - p_{10} + p_{01}}{2}\right) - 0.5H(p_{10}) - 0.5H(p_{01}) \tag{25}$$

where H is the binary entropy, and p_{10} and p_{01} are the crossover probabilities for the transmitted bits of 0 and 1. Let $z = \sqrt{P/4\sigma^2}$ and $\theta = \sqrt{(k-2)/k}$. From Section IV-A

$$p_{10} = 1 - \mathrm{erf}(z),\ p_{01} = \mathrm{erf}(z\theta). \tag{26}$$

It can be easily calculated that

$$\frac{\mathrm{d}H(f(z))}{\mathrm{d}z} = f'(z) \log \frac{1 - f(z)}{f(z)} \tag{27}$$

where $f'(z)$ is the derivative of f with respect to z and log is the logarithm base 2. Then, for $f_1(z) = 0.5(\mathrm{erf}(z\theta) + \mathrm{erf}(z))$

$$\frac{\mathrm{d}H(f_1(z))}{\mathrm{d}z} = \frac{1}{\sqrt{\pi}} \left(e^{-z^2} + \theta e^{-z^2\theta^2}\right) \log\left(\frac{2 - \mathrm{erf}(z\theta) - \mathrm{erf}(z)}{\mathrm{erf}(z\theta) + \mathrm{erf}(z)}\right). \tag{28}$$

Similarly, from the expressions for $f_2(z) = 1 - \mathrm{erf}(z)$ and $f_3(z) = \mathrm{erf}(z\theta)$, the following is obtained:

$$\frac{\mathrm{d}I}{\mathrm{d}z} = \frac{1}{\sqrt{\pi}} \left(e^{-z^2} \log\left(\frac{2 - \mathrm{erf}(z\theta) - \mathrm{erf}(z)}{\mathrm{erf}(z\theta) + \mathrm{erf}(z)} \frac{\mathrm{erf}(z)}{1 - \mathrm{erf}(z)} \right) + \theta e^{-z^2\theta^2} \log\left(\frac{2 - \mathrm{erf}(z\theta) - \mathrm{erf}(z)}{\mathrm{erf}(z\theta) + \mathrm{erf}(z)} \frac{\mathrm{erf}(z\theta)}{1 - \mathrm{erf}(z\theta)} \right) \right). \tag{29}$$

Since $0 < \theta < 1$ and $z > 0$ by definition, it is clear that $\mathrm{erf}(z) > \mathrm{erf}(z\theta)$. Hence, from (29), it can be shown that

$$\left(\frac{2 - \mathrm{erf}(z\theta) - \mathrm{erf}(z)}{\mathrm{erf}(z\theta) + \mathrm{erf}(z)} \frac{\mathrm{erf}(z)}{1 - \mathrm{erf}(z)} \right) > 1, \text{ and}$$

$$\left(\frac{2 - \mathrm{erf}(z\theta) - \mathrm{erf}(z)}{\mathrm{erf}(z\theta) + \mathrm{erf}(z)} \frac{\mathrm{erf}(z\theta)}{1 - \mathrm{erf}(z\theta)} \right) < 1.$$

Then, the following expression is obtained:

$$\frac{\mathrm{d}I}{\mathrm{d}z} = \frac{1}{\sqrt{\pi}} \left(e^{-z^2} \log\left(\frac{2 - \mathrm{erf}(z\theta) - \mathrm{erf}(z)}{\mathrm{erf}(z\theta) + \mathrm{erf}(z)} \frac{\mathrm{erf}(z)}{1 - \mathrm{erf}(z)} \right) - \theta e^{-z^2\theta^2} \log\left(\frac{\mathrm{erf}(z\theta) + \mathrm{erf}(z)}{2 - \mathrm{erf}(z\theta) - \mathrm{erf}(z)} \frac{1 - \mathrm{erf}(z\theta)}{\mathrm{erf}(z\theta)} \right) \right). \tag{30}$$

Let us check if the expressions inside the parentheses are sufficiently close to each other, so that they can be merged into a single logarithm. By equating the terms inside the parenthesis, the following is obtained:

$$\mathrm{erf}^3(z) + \mathrm{erf}^3(z\theta) + 2\mathrm{erf}(z)\mathrm{erf}(z\theta) \approx \mathrm{erf}^2(z)(1 + \mathrm{erf}(z\theta)) + \mathrm{erf}^2(z\theta)(1 + \mathrm{erf}(z)). \tag{31}$$

Assuming $\mathrm{erf}(z) \approx 1$, (31) is correct if $\mathrm{erf}(z\theta)$ is very close to either 0 or 1. Then, (30) is 0 when $e^{-z^2} - \theta e^{-z^2\theta^2} = 0$. As indicated in Section V, these simplifying assumptions leads to analytical formulations quite accurate with the optimal noise power to signal power ratio. Then, the following relation between θ and z is obtained for maximum mutual information:

$$z \approx \sqrt{\frac{1}{1 - \theta^2} \ln\left(\frac{1}{\theta}\right)}. \tag{32}$$

Finally, substituting z and θ values

$$\sigma^2 = \frac{P}{k} [\ln k - \ln(k - 2)]^{-1}. \tag{33}$$

REFERENCES

[1] K. Novoselov, "Graphene: Materials in the flatland (Noberl lecture)," *Angewandte Chemie*, vol. 50, pp. 6986–7002, 2011.

[2] P. Avouris, M. Radosavljevic, and S. Wind, *Carbon Nanotube Elec. and Optoelec.* New York: Springer, 2005, ch. 9, pp. 227–251.

[3] C. Biswas, and Y. H. Lee, "Graphene versus carbon nanotubes in electronic devices," *Adv. Funct. Mater.*, vol. 21, pp. 3806–3826, 2011.

[4] V. Ryzhii, and M. Ryzhii, "Graphene bilayer field-effect phototransistor for terahertz and infrared detection," *Phys. Rev. B*, vol. 79, pp.245311-1–245311-8, 2009.

[5] F. Bonaccorso, Z. Sun, T. Hasan, and A. C. Ferrari, "Graphene photonics and optoelectronics," *Nat. Photon.*, vol. 4, no. 9, pp. 611–622, 2010.

[6] F. Xia, T. Mueller, Y. Lin, A. V. Garcia, and P. Avouris, "Ultrafast graphene photodetector," *Nat. Nanotechnol.*, vol. 4, pp. 839–843, 2009.

[7] B. Gulbahar, and O. B. Akan, "A Communication theoretical modeling of single-layer graphene photodetectors and efficient multireceiver diversity combining," *IEEE Trans. Nanotechnol.*, vol. 11, no. 3, pp. 601–610, May. 2012.

[8] I. F. Akyildiz, F. Brunetti, and C. Blazquez, "Nanonetworks: A new communication paradigm," *Comput. Netw.*, vol. 52, no. 12, pp. 2260–2279, 2008.

[9] Y. Zhang, T. T. Tang, C. Girit, Z. Hao, M. C. Martin, A. Zettl, M. F. Crommie, Y. R. Shen, and F. Wang "Direct observation of a widely tunable bandgap in bilayer graphene," *Nature*, vol. 459, no. 7248, pp. 820–823, 2009.

[10] F. Xia, D. B. Farmer, Y. Lin, and P. Avouris, "Graphene field-effect transistors with high on/off current ratio and large transport band gap at room temperature," *Nano Lett.*, vol. 10, no. 2, ACS Publications, 2010.

[11] I. F. Akyildiz, and J. M. Jornet, "Electromagnetic wireless nanosensor networks," *Nano Com. Net.*, vol. 1, no. 1, p. 3, 2010.

[12] H. Calisto, F. Mora, and E. Tirapegui, "Stochastic resonance in a linear system: An exact solution," *Phys. Rev. E*, pp. 022102-1–022102-4, 2006.

[13] I. Lee, X. Liu, C. Zhou, and B. Kosko, "Noise-Enhanced detection of subthreshold signals with carbon nanotubes," *IEEE Trans. Nanotechnol.*, vol. 5, no. 6, Nov. 2006.

[14] S. Mitaim, and B. Kosko, "Adaptive stochastic resonance in noisy neurons based on mutual information," *IEEE Trans. Neural Netw.*, vol. 15, no. 6, Nov. 2004.

[15] M. D. McDonnell, N. G. Stocks, C. E. M. Pearce, and D. Abbott, "Optimal information transmission in nonlinear arrays through suprathreshold stochastic resonance," *Phys. Lett. A*, vol. 352, pp. 183–189, 2006.

[16] T. Mueller, F. Xia, and P. Avouris, "Graphene photodetectors for high speed optical communications," *Nat. Photon.*, vol. 4, pp. 297–301, May. 2010.

[17] V. Ryzhii, M. Ryzhii, N. Ryabova, V. Mitin, and T. Otsuji, "Terahertz and infrared detectors based on graphene structures," *Infrared Phys. Technol.*, 2010.

[18] M. D. McDonnell, D. Abbott, and C. E. M. Pearce, "An analysis of noise enhanced information transmission in an array of comparators," *Microelectron. J.*, vol. 33, pp. 1079–1089, 2002.

[19] Y. M. Lin, and P. Avouris, "Strong suppression of electrical noise in bilayer graphene nanodevices," *Nano Lett.*, vol. 8, pp. 2119–2125, Aug. 2008.

[20] M. Kocaoglu, and O. B. Akan, "Minimum energy coding for wireless nanosensor networks," in *Proc. IEEE INFOCOM'12*, Orlando, FL, 2012.

[21] M. Kocaoglu, and O. B. Akan, "Minimum energy channel codes for nanoscale wireless communications," *IEEE Trans. Wireless Commun.*, vol. 12, no. 4, pp. 1492–1500, Apr. 2013.

[22] C. E. Shannon, "A mathematical theory of communication," *Bell Syst. Tech. J.*, vol. 27, pp. 379–423, Oct. 1948.

[23] A. Leon-Garcia, *Probability and Random Processes for Electrical Engineering*. Reading, MA: Addison-Wesley, 1989.

[24] J. M. Kahn, and J. R. Barry, "Wireless infrared communications," *Proc. IEEE*, vol. 85, pp. 265–298, Feb. 1997.

Murat Kocaoglu (S'06) received the B.S. degree in electrical and electronics engineering with a minor in physics from Middle East Technical University, Ankara, Turkey, in 2010, and the M.S. degree in electrical and electronics engineering from the Next-Generation and Wireless Communications Laboratory, Koc University, Istanbul, Turkey, in 2012. He is currently working toward the Ph.D. degree at The University of Texas at Austin, Austin, TX, USA.

His current research interests include graphical models, learning theory, and coding theory.

Burhan Gulbahar (M'13–SM'14) received the B.S. and M.S. degrees in electrical and electronics engineering from Bilkent University, Ankara, Turkey, in 1999 and 2002, respectively, and the Ph.D. degree in electrical and electronics engineering from Koc University, Istanbul, Turkey, in January 2012.

He was a Research Assistant with the Next-Generation and Wireless Communications Laboratory, Koc University. He is currently an Adjunct Assistant Professor at the Department of Electrical and Electronics Engineering, Ozyegin University, Istanbul, and a Researcher at Research Group, Vestel Electronics Inc., Manisa, Turkey. His current research interests include nanoscale communications, visible light communications, graphene and carbon nanotube communication networks, wireless sensor networks, quantum communications, and consumer electronics for smart home architectures.

Ozgur B. Akan (M'00–SM'07) received the Ph.D. degree in electrical and computer engineering from the Broadband and Wireless Networking Laboratory, School of Electrical and Computer Engineering, Georgia Institute of Technology, Atlanta, GA, USA, in 2004.

He is currently a Full Professor with the Department of Electrical and Electronics Engineering, Koc University, Istanbul, Turkey, where he is also the Director of the Next-generation and Wireless Communications Laboratory. His current research interests include wireless communications, nanoscale and molecular communications, and information theory.

Dr. Akan is an Associate Editor of the IEEE TRANSACTIONS ON COMMUNICATIONS, IEEE TRANSACTIONS ON VEHICULAR TECHNOLOGY, the *International Journal of Communication Systems* (Wiley), the *Nanocommunication Networks Journal* (Elsevier), and the *European Transactions on Technology*.